Electrical transport in a superconducting niobium nitride ultrathin granular film: A disordered two-dimensional Josephson-junction array

Mark W. Johnson* and Alan M. Kadin
Department of Electrical Engineering, University of Rochester, Rochester, New York 14627
(Received 22 May 1997)

A granular ultrathin niobium nitride (NbN) film, 10 nm thick, was patterned into long narrow lines ranging from 1 to 20 μm wide. The film can be modeled as a two-dimensional array of Josephson junctions, with junctions on the scale of 30 nm, as supported by dc and rf electrical measurements (resistance, inductance, and critical current) in the absence of an applied magnetic field, both above and below the superconducting critical temperature $T_c \sim 6.5$ K. The analysis confirms the standard model of vortex unbinding in a regular two-dimensional junction array, with no free parameters. However, atomic-force-microscopy topographic images show substantial inhomogeneity, and this is also evident in reduced values of critical current density J_c in the narrowest lines. These are consistent with a simple model of film variations up to the 1 μm scale. Finally, observations are reported of an anomalous decrease in the rf kinetic inductance of the films with increasing dc current, which may also be a consequence of the Josephson-junction array. [S0163-1829(98)05606-9]

I. INTRODUCTION

There have been a considerable number of investigations into two-dimensional arrays of Josephson junctions (2D JJ arrays), from both experimental and theoretical perspectives.[1–12] In addition to uniform junctions in a regular lattice, effects of local defects and disorder have also been addressed.[13–23] In addition, there have been many studies of granular and disordered, superconducting ultrathin films,[24–28] which in certain respects can be modeled as disordered 2D JJ arrays. A diverse set of physical phenomena involving superconducting vortices can be studied in such systems, including unbinding of vortex-antivortex pairs and vortex-lattice melting.

Here we present a systematic study of the transport properties of ultrathin granular niobium nitride (NbN) films in zero applied magnetic field, and show that these may indeed be modeled as 2D JJ arrays. This is despite a significant degree of inhomogeneity on several length scales, as shown by topographic images obtained by atomic-force microscopy (AFM). In addition to the resistive transition above the superconducting critical temperature T_c, we also measure the critical current and the rf kinetic inductance in the superconducting state below T_c. These are all determined for the same film, patterned into lines of different widths. This enables us to explore effects related to scaling and inhomogeneity, which have not previously been fully addressed.

II. EXPERIMENT

A. Sample fabrication and characterization

The NbN samples reported here were designed and fabricated by the TRW Space and Technology Group in Redondo Beach, CA. The 10 nm thick film was deposited on an unoxidized Si wafer using reactive dc magnetron sputtering in an argon/nitrogen plasma.[29] This was patterned using argon ion etching into a series of meander lines of different widths (1, 2, 5, 10, and 20 μm) but constant total area (0.01 mm^2), all contained on the same 0.5 cm square chip (see Fig. 1). The leads on-chip were also NbN, but a much thicker film with a higher value of T_c. It is noteworthy that these ultrathin films are surprisingly robust; they have not degraded in ambient conditions in air over a period of several years.

One sample was selected for examination of microstructure by atomic-force microscopy (see Fig. 2), using a Digital Instruments Nanoscope AFM (at Eastman Kodak Research Laboratory). This clearly shows a highly granular structure, with a wide range of apparent grain sizes down to about 10 nm, comparable to the thickness. In addition, there appears

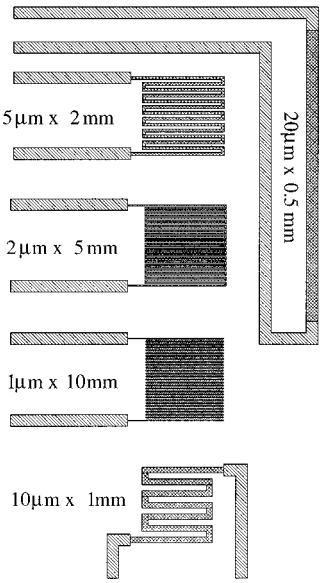

FIG. 1. Layout of patterned NbN film (detail) on Si wafer. The cross-hatched meander lines are the ultrathin NbN (10 nm thick) with $T_c \approx 6.5$ K, which are the subject of the present study; the single-hatched lines (20 μm wide) are thicker NbN leads with $T_c = 11$ K. Lines shown have dimensions 20 μm wide$\times$0.5 mm long, 10 μm$\times$1 mm, 5 μm$\times$2 mm, 2 μm$\times$5 mm, and 1 μm$\times$10 mm, each for a total area of 0.01 mm^2.

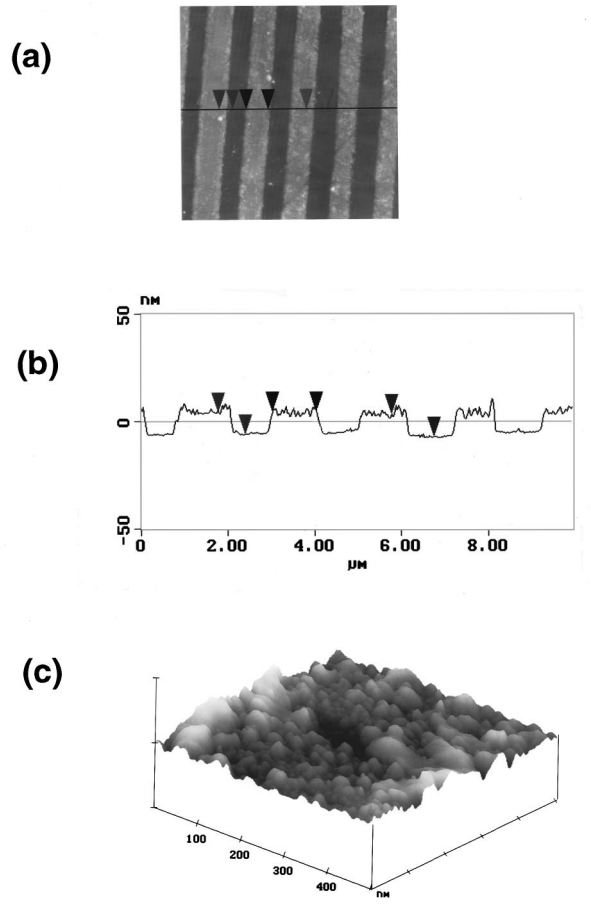

FIG. 2. Atomic-force-microscope images (reprinted with permission of Eastman Kodak Company) of patterned ultrathin NbN film on Si wafer, made using Digital Instruments NanoScope AFM in tapping mode. (a) Image of portion of 1 μm wide meander line (10 μm full scale), with NbN bright on dark Si background. (b) Line scan of the image in (a), showing film thickness and surface roughness. (c) Close-up view of NbN line, (100 nm/div. horizontal scale, 30 nm/div. vertical scale), showing a random distribution of grains on $\sim$30 nm scale, but with clusters of grains on larger scales.

to be some clustering of grains on a larger scale (up to about 1 μm), so that despite the accurate microlithography, one would expect to observe measurable effects of this inhomogeneity, particularly for the narrower lines.

B. Electrical measurements

The chip was mounted in a ceramic chip carrier in vacuum, thermally anchored to a temperature-controlled stage in a liquid helium dewar, with a silicon diode thermometer and a Lake Shore Cryotronics controller. Electrical contact was made to a set of gold bonding pads, using ultrasonically bonded 25 μm Al wires. We will focus primarily on the measurements from four lines on the same chip: 2 μm wide$\times$5 mm long, 5 μm wide$\times$2 mm long, 10 μm$\times$1 mm long, and 20 μm wide$\times$0.5 μmm long. These measurements were taken during a recent study of the photoresponse of these structures to visible and infrared radiation.[30–32] No external magnetic field was applied, and no effort was made to screen out the earth's magnetic field ($\approx$0.5 G). (This small background field does not significantly alter the results, as discussed in Sec. IV.) For dc measurements, current was supplied using either a battery or a Keithley model 224 programmable current source, and the voltage was measured using a Keithley model 182 sensitive digital voltmeter. rf measurements (for kinetic inductance) were made using an HP-8753A vector network analyzer connected across the meander line with a 50 Ω coaxial line.

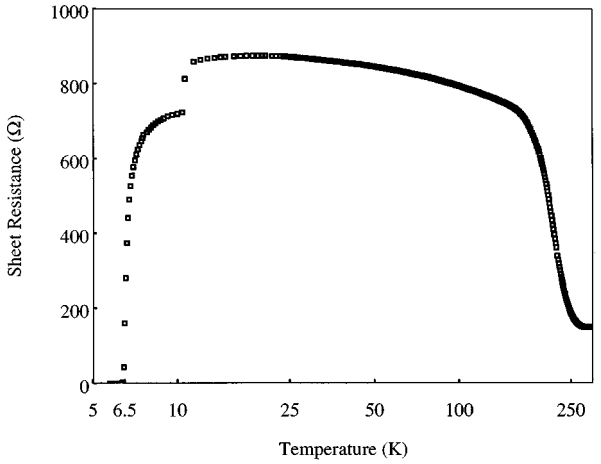

FIG. 3. Temperature dependence (on a log scale) of the dc sheet resistance $R_s = R/100$ of ultrathin NbN line, 10 μm wide$\times$1 mm long. Note the Si carrier freezeout at 200 K, the drop at 11 K due to the thicker NbN leads, and the approach to $R = 0$ at 6.5 K.

In Fig. 3, we show the dc resistance vs temperature for a meander line 10 μm$\times$1 mm long. Note that the resistance rises sharply as the temperature is cooled below 250 K. The room-temperature resistance reflects the shunt conductance from the NbN line through the Si substrate (the oxide was deliberately etched off this sample before depositing the NbN). The carriers in this intrinsic semiconductor freeze out below around 200 K, leaving the resistance of the NbN line itself. Below 200 K, the temperature coefficient of resistance is still slightly negative, showing partially activated conduction indicative of weakly coupled grains. The low-temperature behavior exhibits two distinct critical temperatures. The higher T_c, at 11 K, is due to the thick ($\approx$100 nm) NbN bias lines. This is somewhat below that of ideal NbN (up to 17 K), and may reflect the granular nature of the material and/or nonideal stoichiometry.[33–35] The lower T_c, at 6.5 K, is that of the ultrathin meander line structure, and is depressed further due to being so thin (10 nm). The peak resistivity of this ultrathin film at the peak (at 9 K) is about 750 $\mu\Omega$ cm, much greater than that of pure NbN, and greater than the maximum metallic resistivity $\sim$200 $\mu\Omega$ cm, due to the granular microstructure.

Figure 4 shows the critical current density for several lines on the same chip, as a function of temperature. As illustrated schematically in the inset, I_c is defined by a sharp rise in voltage in a curve that is typically hysteretic due to self-heating. Because of the hysteresis, it was important that the input and output lines be properly filtered to prevent premature switching by digital noise that is often present in modern instruments. Note that J_c is somewhat reduced for the narrower lines, and that T_c (the extrapolation to $J_c = 0$) is

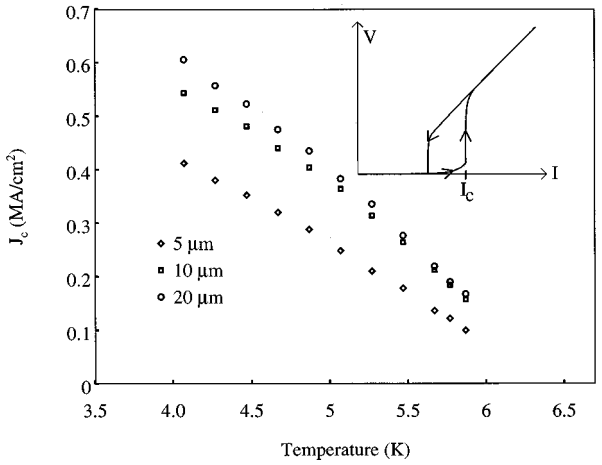

FIG. 4. Temperature dependence of the critical current density J_c for NbN lines of several widths (as labeled). The critical current is defined here as the current at which the voltage starts rising sharply (and generally hysteretically), as indicated schematically in the inset.

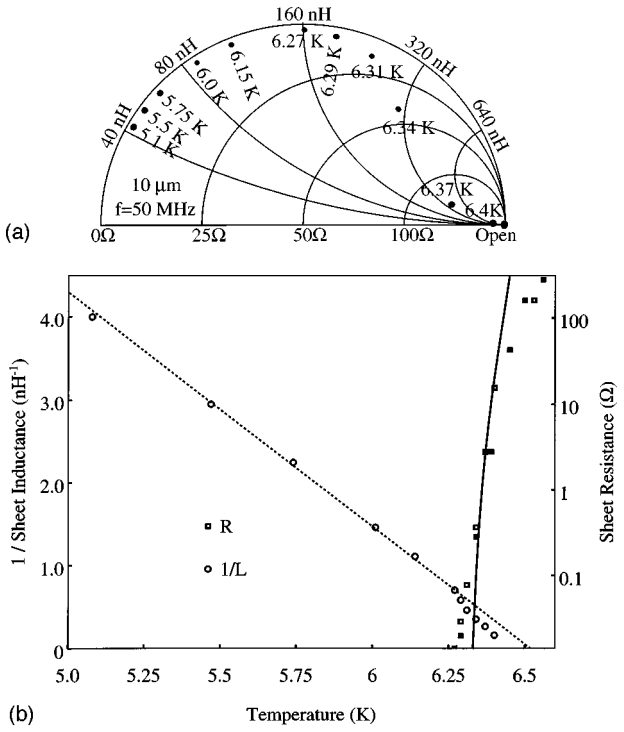

FIG. 5. rf impedance measurements of 10-μm wide NbN line in superconducting state, using reflection measurements at 50 MHz, for zero dc bias current and small rf current. (a) Smith chart representation of impedance values, for T as labeled. (b) Temperature dependence of R_s and $1/L_s$ (per square), from rf impedance data in (a). Values of L_s have been corrected for an estimated 13 $nH = \mu_0 * (1\text{ cm})$ associated with series magnetic inductance of leads. Also included (solid squares) are dc resistance data, confirming the proper calibration and consistency of the rf impedance. Note that L_s appears to diverge at about 6.5 K, while R_s goes to zero at about 6.3 K. The theoretical lines for the kinetic inductance and the ''universal resistive transition'' of a 2D superconductor (both for a normal sheet resistance of 750 Ω) are also shown.

also slightly depressed. We believe that both are real effects related to inhomogeneity, as discussed further in a later section.

To determine the kinetic inductance of the film,[36] we measured the complex reflection coefficient $\rho = V_r / V_i$ of an rf signal from the meander line, treating the meander line as a lumped element (valid at the frequencies of interest). This is a standard measurement using an rf vector network analyzer, and permits determination of the impedance Z using the expression $Z/Z_0 = (1+\rho)/(1-\rho)$, where $Z_0 = 50\ \Omega$ is the characteristic impedance of the transmission line leading to the device. This is the same transformation that forms the basis of the Smith Chart. This provides a highly accurate measurement of Z when it is within a factor of 10 of Z_0, so that the operating frequency (typically 1–100 MHz) was chosen to make $|Z|$ on the same order as Z_0. We were also able to compensate for the phase shift in the input line through a standard calibration procedure built into the network analyzer. The calibration was verified by ensuring that the meander line appears open ($Z \sim 100\ \text{k}\Omega \gg 50\ \Omega$) when in the fully normal state. In the superconducting state, $Z = R + i\omega L$, where R includes any series resistance in the wire bonds and contacts (believed to be negligible), $L = L_m + L_k$ includes both the total magnetic inductance and the kinetic inductance of the superconducting film, and $\omega = 2\pi f$ is the angular frequency. It was critical to reduce the signal power so that it was truly the small signal impedance that was being measured. This corresponded typically to a current amplitude of a few μA or less. The complex value of ρ is shown in Fig. 5(a) for a range of temperatures near T_c, for the 10 μm NbN line at 50 MHz, together with the Smith Chart lines that identify R and L. The inductance is diverging as T_c is approached, and R begins to rise sharply close to T_c. We estimate an excess contribution to the magnetic inductance $\sim \mu_0^*(1\text{ cm}) = 13$ nH, associated with the wire bonds and leads, and we subtract this off the measured inductance values for all the lines. This is a significant correction for the wide lines at low temperatures; otherwise, it is a small effect. In Fig. 5(b), the values (per square) of $1/L_s$ and R_s thus inferred are plotted against T. Note that $1/L$ appears to extrapolate to about 6.5 K, while R goes to zero at about 6.3 K. This difference is due to 2D vortex effects, as described in the next section. We also examined the rf reflection coefficient for fixed temperature as a function of dc current (Fig. 6), and found that $L(I)$ exhibits a surprising decrease as I approaches I_C.

III. DATA ANALYSIS

A. Uniform JJ array model

Consider a regular 2D JJ array, of identical Josephson junctions, each with critical current I_{c0} and normal state resistance R_n, separated by a distance a, as shown in the inset of Fig. 7. (We assume that the junction capacitance can be neglected.) From the supercurrent relation $I = I_{c0}\sin\phi$ and the voltage relation $V = (\hbar/2e)d\phi/dt$, we obtain in the standard way the Josephson inductance for small ac currents (and $I_{dc} = 0$): $L_j = \hbar/(2eI_{c0}\cos\phi) = \hbar/(2eI_{c0})$. If current flow is uniform across the width w of the array, then the total critical current of the array is $I_c = (w/a)I_{c0}$ and the kinetic inductance per square (the ''sheet inductance'') is $L_s = L_j$ (neglecting renormalization effects associated with vortices).

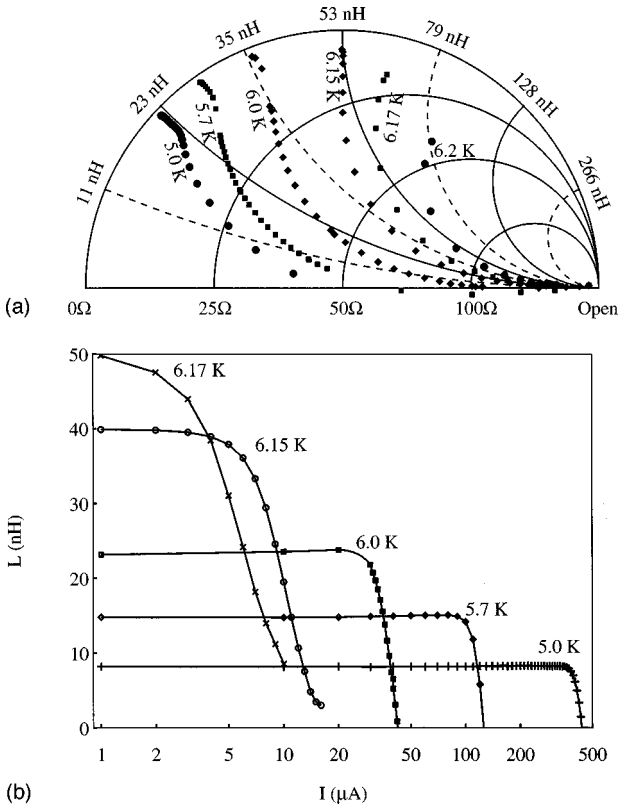

FIG. 6. rf impedance measurements of 20-μm wide NbN line, using reflection measurements at 150 MHz, as the dc bias current is increased for several fixed values of temperature. (a) Smith chart representation, for T as labeled. (b) Corresponding current dependence $L(I)$.

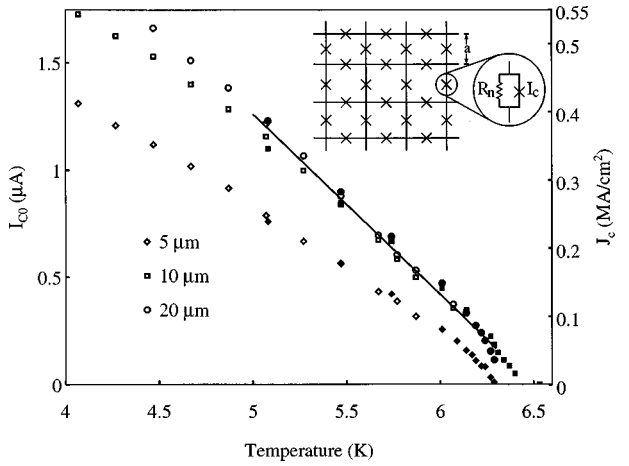

FIG. 7. Temperature dependence of single-junction critical current $I_{c0}(T)=\hbar/2eL_s$ inferred from rf impedance measurements, for NbN lines of several widths (solid symbols). The inset shows a schematic of the uniform 2D Josephson-junction array model on a square lattice of constant a. Each junction is assumed to have shunt resistance R_n, critical current I_{c0}, and Josephson inductance $L_j=\hbar/2eI_{c0}$. The solid line follows from the theoretical dependence of an ideal Josephson junction, for $R_n=750\ \Omega$ (the same as the sheet resistance of the film at 9 K). Also plotted (open symbols) are the measured values of total J_c from Fig. 4, assuming a single value of the lattice constant $a=I_{c0}/J_c d=32$ nm.

We refer to kinetic inductance, since this is conventional for a thin film, but the basic physical mechanism is the same in either case.

The current distribution is determined in general by a balance between the kinetic inductance and the magnetic inductance. As shown by a more complete analysis,[3] the characteristic length is the effective transverse penetration depth $\lambda_\perp=L_s/\mu_0=\hbar/(2e\mu_0 I_{c0})$. If the film width $w\ll\lambda_\perp$, then the current distribution should be uniform and we can generally neglect the magnetic portion of the inductance. As indicated in Fig. 5, the measured inductance is large and is strongly dependent on temperature near T_c. This confirms our belief that it is dominated by the kinetic (or Josephson) inductance, since the magnetic inductance should be independent of temperature. Taking a typical sheet inductance of order 1 nH for the line, we obtain $\lambda_\perp\approx 1$ mm, and even for the lowest T, $\lambda_\perp>200\ \mu$m, much greater than any of the linewidths in the samples we have studied. So our assumption of uniform current flow should be valid in all cases here. We can also compare $\lambda_\perp$ to the corresponding quantity $\lambda(T)^2/d$ for a thin nongranular film, where $\lambda(T)$ is the bulk magnetic penetration depth.[37] A typical value for $\lambda(T=0)$ for bulk NbN is 0.2 μm, which would give a value of $\lambda_\perp\approx 4\ \mu$m. Although this would be somewhat enhanced close to T_c in the dirty limit, the measured values clearly indicate that we are well into the regime of weakly coupled grains.

From our measurements of L_s, we can determine $I_{c0}=\hbar/2eL_s$, as is done in Fig. 7 for several different widths. By superimposing this with our direct measurements of $I_c=(w/a)I_{c0}$, we can infer the value of the array lattice scale a. The best single-parameter fit for the entire data set is $a=32$ nm, which is quite reasonable given the nature of the films and the observed topography. We can also compare the temperature dependence of I_{c0} with that theoretically expected for a tunnel junction[37] with $T_c=6.5$ K: $I_{c0}=(\pi\Delta/2eR_n)\tanh(\Delta/2kT)$, where $\Delta(T)$ is the BCS gap function and $\Delta(0)=1.76kT_c$. The line fit to the data (shown in Figs. 7 and 5(b), corresponding to the linear behavior close to T_c), is for $R_n=750\ \Omega$, the measured value of sheet resistance in the normal state at 9 K. It is interesting to note that this is not a unique indicator of a 2D JJ array; a homogeneous 2D superconducting film in the dirty limit would exhibit exactly the same dependence of L_s on T and R_n. However, I_c would go as $(T_c-T)^{1.5}$ for a homogeneous film, in contrast to the linear behavior, appropriate to a junction, observed in Fig. 4. So it would appear that our picture of a 2D JJ array is a self-consistent representation of this granular NbN film.

Another hallmark of 2D superconductivity is the Kosterlitz-Thouless (KT) vortex-unbinding transition.[37–40] Within the KT picture, local superconducting order forms below the mean-field critical temperature T_{c0}, but unbound vortex excitations cause residual resistance until the lower critical temperature $T_c=T_{\rm KT}$, below which all such vortices are bound in vortex pairs, and the linear resistance goes to zero. $T_{\rm KT}$ is given by the following self-consistent expressions.

$$k_B T_{\rm KT}=(\pi/2)E_j=I_{c0}\Phi_0/4=\Phi_0^2/8\pi L_s, \qquad (1)$$

where $E_j=\hbar I_{c0}/2e$ is the Josephson coupling energy and $\Phi_0=h/2e$ is the flux quantum. If we estimate the $T_{\rm KT}=6.3$ K from Fig. 5 as the temperature at which R drops sharply, we obtain $I_{c0}=0.17$ μA and $L_s=2$ nH, which indeed occurs at $T=6.3$ K, close to the prediction. Furthermore, the difference between T_{c0} and $T_{\rm KT}$ can be given in terms of the normal-state sheet resistance R_n (Ref. 38), which for $T_{\rm KT}$ close to T_{c0} takes the form

$$(T_{c0}-T_{\rm KT})/T_{c0}\approx R_n/24\ \ k\Omega. \tag{2}$$

Taking $R_n=750\ \Omega$ gives a temperature difference of 0.2 K, suggesting that $T_{c0}=6.5$ K. This is close to the temperature at which L_s appears to be diverging in Fig. 5, and the temperature at which R appears to be going to zero on the gross resistance scale in Fig. 3. Furthermore, the shape of the resistive transition for a variety of 2D superconductors tend to follow a ''universal resistance curve''[40] in the tail of the resistance between $T_{\rm KT}$ and T_{c0}, which takes the form:

$$R/R_n=C_0X\ \exp(-C_1/\sqrt{X-1}), \tag{3}$$

where $X=(T/T_{\rm KT})(T_{c0}-T_{\rm KT})/(T_{c0}-T)$ is the scaled temperature, $C_0=1.7$, and $C_1=4.9$. This is plotted along with the resistance data in Fig. 5 (using the values $R_n=750\ \Omega$, $T_{c0}=6.5$ K, and $T_{\rm KT}=6.3$ K,), and provides a reasonable fit given the lack of free parameters. (The broadening at the lower end of the resistive tail may be a consequence of inhomogeneity.) Overall, this is quite consistent with the presence of a KT transition.

Several researchers[24–28] have obtained additional evidence of the KT transition and vortex interactions by examining the nonlinear I-V curves near and below T_c, which reflect the presence of nonequilibrium vortices created by thermally activated depairing of bound vortex pairs in the presence of large currents.[39] In fact, the behavior of the exponent $a(T)$ in curves that follow $V\sim I^{a}(T)$ (i.e., straight lines on a log-log plot) generally provides the most direct and unequivocal evidence for the KT transition. Unfortunately, we did not undertake a systematic study of these I-V curves in the present case, but some curves well below the transition [as in Fig. 9(a)] exhibit qualitatively the expected behavior.

We can also consider the current dependence of the kinetic inductance $L_s(I)$ within the context of a 2D JJ array. To the extent that we identify L_s with the local Josephson inductance we have

$$L_s(I)=\frac{\hbar}{2eI_c\cos\phi}=\frac{\hbar}{2e[I_c^2-I^2]^{0.5}}=\frac{L_s(0)}{[1-(I/I_c)^2]^{0.5}}, \tag{4}$$

suggesting a weak divergence of L_s as I approaches I_c. An analysis for a superconducting thin film using Ginzburg-Landau theory also yield an increase in L_s.[41] Self-heating would also yield an increase. In sharp contrast, the observed dependence shows a *decrease* in L_s as I approaches I_c [see Fig. 6(b)]. Although we do not have a firm understanding of this effect, we suspect that it can be accounted for in terms of the 2D JJ array model. Two factors must be considered in this analysis: thermal fluctuations and the ac Josephson effect.

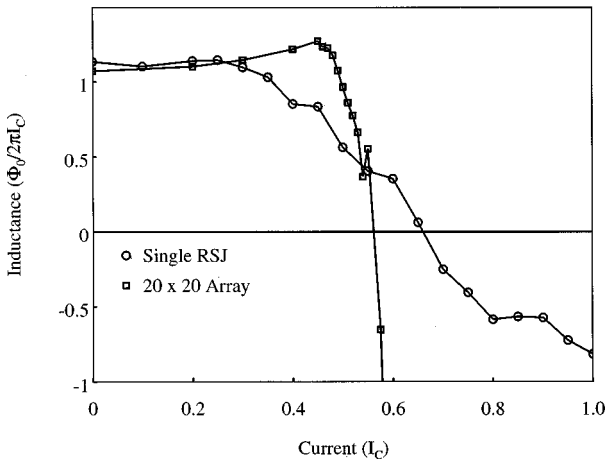

FIG. 8. Simulated Josephson inductance as a function of dc bias current, for single resistively shunted junction and for a 20×20 array, for small ac current at frequency ω. $T=0.25$ (normalized to $\hbar I_{c0}/2ek$) and $\omega=0.01$ (normalized to $2eI_{c0}R_n/\hbar$). Note that both curves exhibit L decreasing with increasing I as seen in experimental data in Fig. 6.

First, we are operating at temperatures where thermal fluctuations are distinctly important; the thermal energy $kT_{\rm KT}$ is comparable to the Josephson coupling energy E_j. When thermal fluctuations are added, simulations for a single JJ do indeed show a decreasing L_j associated with large increasing I and increasing R (Fig. 8). The second consideration is the ac Josephson effect, in which an external ac signal can phase lock the internal junction oscillation on the Shapiro step in the I-V characteristics at a voltage $V=n\hbar\omega/2e$. This is associated with a strongly varying (and generally negative!) effective inductance across the step.[42] It is worth noting in this regard that the Josephson frequency corresponding to 50 MHz (a typical rf measurement frequency) is 0.1 μV. Given a series array of 30,000 junction rows for the 10 μm line (1 mm/32 nm), this gives a total voltage of 3 mV, which is indeed a typical voltage in the range where L_s decreases. We do not see Shapiro steps (giant or otherwise) in our I-V characteristics (at least at the very low rf amplitudes we use), but thermal fluctuations and the randomness of the array could serve to wash these out. Finally, we have carried out a preliminary simulation of a regular 20×20 JJ array of resistively shunted junctions,[32] using an algorithm similar to that in Ref. 11. Thermal fluctuations are incorporated using a Gaussian random noise current corresponding to the Johnson noise in the shunt resistor of each junction. As illustrated in Fig. 8, this simulation also shows an inductance that decreases with increasing current in a way that is qualitatively similar to that in Fig. 6(b). This suggests that Josephson effects in the junctions of the array (or equivalently, coherent vortex dynamics) may be responsible for this effect. But clearly, further analysis is needed to show this more conclusively.

B. Width scaling and inhomogeneity

One of the unique aspects of our set of samples is the wide range of linewidths in otherwise identical films, each with the same area $A=wl$. For this reason, we chose to examine how I, V, and R should be expected to scale with

the width w. For an ideal macroscopically homogeneous film, with $w \gg a$, with uniform current flow ($w \ll \lambda_\perp$), we would expect that $I_c = J_c w d$, where J_c is an intrinsic quantity independent of w. Unfortunately, this scaling was not obeyed in our narrowest films, for reasons of inhomogeneity that we will discuss below.

However, let us first examine the scaling of voltage that one would expect for a homogeneous film or array in the superconducting state, where all resistance is associated with moving vortices. For the voltage $V(J)$, we should distinguish the two limits associated with recombination of generated vortices. In the limit that the vortices move off the edge before recombining in the film, each vortex pair creation is equivalent to a single vortex moving across the film, which corresponds in turn to an integrated voltage pulse of magnitude Φ_0. So if the areal density of vortex pair generation is $\Gamma(J)$, then for the time-average voltage we have

$$V(J) = \Phi_0 \Gamma(J) l w \sim A \quad \text{(edge limit)}. \tag{5}$$

In the other limit that the vortices recombine within the film, moving an average distance $x \ll w$, each vortex generation event leads on average to a voltage pulse of integrated magnitude $\Phi_0 x/w$, so that the average voltage is now

$$V(J) = \Phi_0 \Gamma(J) l w (x/w) \sim l = A/w \quad \text{(area recombination limit)}. \tag{6}$$

The scaling should in principle help us to identify clearly the relevant regime.

It may be useful in this regard to estimate the effective free vortex density. The Bardeen-Stephen model for flux flow in a thin superconducting films states that $R/R_n = 2\pi\xi^2 N_v$, where ξ is the superconducting coherence length in the film. For a square JJ array, the role of $2\pi\xi^2$ is taken by a^2,[7] so we have $N_v = R/(a^2 R_n)$. For our NbN films, a typical film sheet resistance in the relevant regime is 0.1 Ω, as compared with a normal-state resistance of order 750 Ω. This yields $N_v \approx 10^7$ cm^{-2}, or one vortex per 10 000 unit cells, corresponding to an intervortex distance of order $100a$. For comparison, the 10 μm wide line is $300a$ wide. This might seem to be in the sparse vortex limit, where the vortices would move transversely to the edge rather than recombining within the film.

In order to compare with experimental data on $V(J)$, we first have to face the lack of scaling of J_c. Putting aside for the moment the question of why this is the case, we can naively ''rescale'' J in proportion to the measured J_c, at least at a single temperature. Then, we can compare $V(J_{\rm corr})$ for the various widths, and see whether it scales more like the edge or recombination limit. This is shown in Fig. 9, for the 2, 5, 10, and 20 μm lines at 5.5 K, both before and after J correction (which amounts to a horizontal shift of up to a factor of 4 for the 2 μm line). The results show that $V(J_{\rm corr})$ becomes consistently larger as the lines become narrower, with a width dependence that goes as $1/w$ or even stronger. It appears to be clearly inconsistent with the edge limit, where we would expect that $V(J)$ would be constant for lines with the same total area A. This apparent area recombination occurs despite the rather sparse density of vortices, as estimated above.

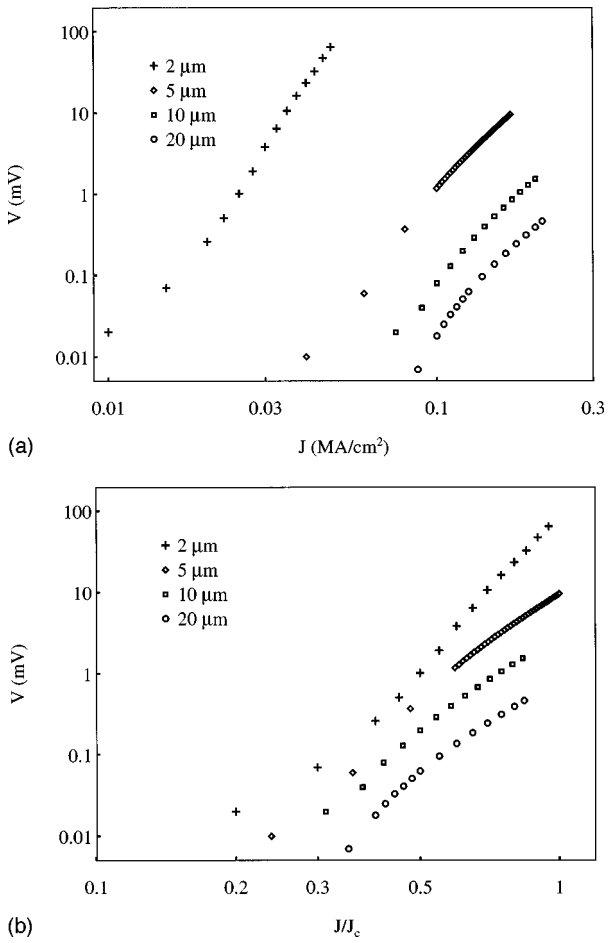

FIG. 9. Nonlinear $V(J)$ for NbN lines of various widths, in the superconducting state at $T = 5.5$ K. (a) Raw data $V(J)$. (b) Voltage data from (a), plotted against J/J_c (taken from Fig. 4). The area recombination model predicts $V \sim 1/w$ (close to that observed), whereas the edge model predicts that V is independent of w.

Most of the results above are quite consistent with a homogeneous 2D JJ array model. How can we explain the lack of scaling of J_c? On first reflection, one might suspect that the patterning was systematically inaccurate, or damaged the superconductivity near the edges of the line. However, examination using a microscope and AFM have shown no evidence of such damage or inaccuracy. An alternative explanation that we think is more likely is the effect of inhomogeneity. Certainly, the AFM images do not give the impression of great regularity in the grain microstructure, on scales from 10 nm up to even 1 μm. Let us focus on inhomogeneity in J_c on a characteristic scale much greater than the typical grain size—for example, $b \sim 1$ μm. This might be due to clusters of grains or some other phenomena, but let us simply assume that J_c has some normal probability distribution with a characteristic spread δJ over this length scale. Qualitatively, if w becomes comparable to b, we would expect greater variation in I_c along the length, and since the measured I_c corresponds to the minimum along the length, this picture would be expected to yield a reduced effective J_c in narrower lines.

Let us now develop this simple picture in more detail. We first discretize the model, by dividing up the film into square plaquettes of size $b \times b$, and assume that the critical current

is a constant for each plaquette, but may vary randomly (with no spatial correlations) between adjacent plaquettes. We can express this quantitatively by stating that the probability that the critical current density for a given plaquette falls between J and $J+dJ$ is

$$P(J)=\frac{dJ}{\delta J\sqrt{\pi}}\exp\left[\frac{-(J-J_{c0})^2}{\delta J^2}\right]. \tag{7}$$

For a film of width w, there will be w/b plaquettes across its width. Each row along the width of the film will have its own critical current, equal to the sum of the critical currents of the individual plaquettes. The distribution of I_c among the rows takes the form

$$P(I_c)=\frac{dI_c}{\delta Jd\sqrt{\pi wb}}\exp\left[\frac{-(I_c-I_{c0})^2}{wbd^2\delta J^2}\right], \tag{8}$$

where $I_{c0}=J_{c0}wd$. This follows from the equation above, and the fact that the sum of N Gaussian random variables of variance σ^2 is itself a Gaussian random variable with variance $N\sigma^2$.

Now, the total critical current of the film should be taken as that of the row with the smallest critical current. This is of course an approximation; it assumes that the current can redistribute itself as needed from one row to the next. Such an approximation will consistently overestimate the critical current, but it will serve for the present. The probability that a given row has critical current greater than a particular value $I_{c1}<I_{c0}$ is then the integral of the above equation from I_{c1} to infinity, or

$$P(I_c>I_{c1})=0.5+0.5\ \mathrm{erf}\left(\frac{I_{c0}-I_{c1}}{\delta Jd\sqrt{wb}}\right), \tag{9}$$

where erf is the standard error function $\mathrm{erf}(x)=(2/\sqrt{\pi})\int_0^x\exp(-y^2)dy$. For a film L/b rows long, the probability that all rows have critical current greater than I_{c1} is this probability raised to the L/b power. Within this simple model, we choose the effective I_c for the line such that this probability has the somewhat arbitrary value 50%, as the solution to the following equation:

$$0.5=\left[0.5+0.5\ \mathrm{erf}\left(\frac{I_{c0}-I_c}{\delta Jd\sqrt{wb}}\right)\right]^{L/b}$$
$$=\left[0.5+0.5\ \mathrm{erf}\left(\frac{J_{c0}-J_c}{\delta J\sqrt{w/b}}\right)\right]^{L/b}, \tag{10}$$

where the latter expression gives the effective critical current density J_c for comparing lines of different widths. We use δJ, J_{c0} and b as fitting parameters. We have not carried out a systematic optimization of these parameters, but using reasonable values $b=2\ \mu$m, $J_{c0}=0.34$ MA/cm^2 (at 5.5 K), and $\delta J/J_{c0}=35\%$, we can obtain a good fit in Fig. 10 for lines that are 2, 5, 10, and 20 μm wide. Of course, using 3 adjustable parameters to fit 4 experimental points does not provide strong evidence for this physical picture, but still it is encouraging. Furthermore, the topographic pictures (Fig. 2) do suggest that clusters of grains on the 1 μm scale appear to be present in these films. However, equally good fits can also be obtained using a smaller value of b together with an increased width of the distribution $\delta J/J_{c0}$. It is quite possible, therefore, that inhomogeneity in J_c is present over a wide range of length scales; the morphology of Fig. 2 would certainly seem to suggest this.

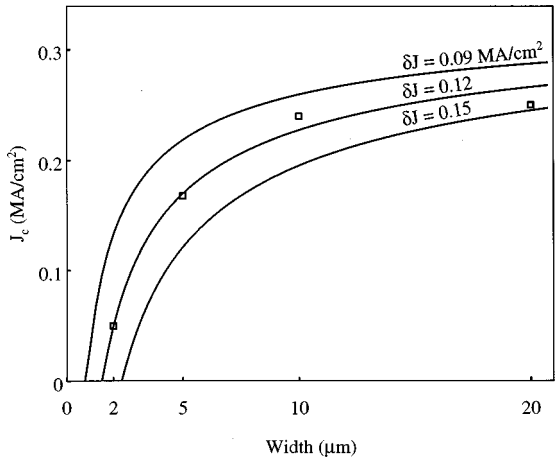

FIG. 10. Effective critical current density at $T=5.5$ K for NbN lines of various widths, compared to fitted predictions (solid lines) of simple inhomogeneity model as described in the text, for parameters $J_{c0}=0.34$ MA/cm^2, $\delta J=0.09$, 0.12, and 0.15 MA/cm^2, and plaquette scale $b=2\ \mu$m.

IV. DISCUSSION AND CONCLUSIONS

At this point, we have two complementary models for the properties of these NbN granular films. In one, we have a uniform 2D array of Josephson junctions, each with $T_c=6.5$ K and $R_n=750\ \Omega$, separated by a scale of 32 nm. In the other, we have a random array of grains with a broad distribution of intergrain coupling and sizes. It is perhaps remarkable that this highly disordered junction array apparently fits so well to the theory for a perfectly regular 2D array.

Such a picture of inhomogeneity might also explain the apparently reduced values of T_c in the narrower lines. The local T_c for a very small, weakly coupled grain is likely to be somewhat depressed. If there are small variations in T_c on the 1 μm scale, perhaps correlating with variations in grain size or intergrain coupling energy, then the effective T_c for the line would behave in much the same way as would I_c; it would be the minimum T_c for any row in the line. In contrast, similar small variations in local resistance would be much less evident in a macroscopic measurement, since the total resistance is just the sum of the resistances for each row. Still, it may be significant that for the 5 μm line, both J_c and $I_{c0}=\hbar/2eL_s$ (Figs. 4 and 7) are depressed in the same way. This is not simply due to the depression of T_c; the slopes are significantly depressed as well. Both of these may represent averages over distributions, but it is not at all clear that an average of inhomogeneous critical currents should behave the same way as an average over impedances.

A possible alternative mechanism for the reduced values of J_c in narrower lines might follow from a consideration of the vortex generation rate. If the current flow is uniform, then at $J=J_c$, vortex generation should occur at a high rate

both within the film and at the edge. Edge generation would be expected to be more dominant in narrower films. If such edge generation were to occur at a reduced value of J, this would tend to reduce the apparent value of J_c. However, it is not clear that this could account for a depressed T_c, or how it would affect L_s.

One factor that we have completely neglected is the effect of junction capacitance, and related single-electron charging effects. In terms of classical effects of capacitance on a single Josephson junction, the capacitance is significant only if the RC time is greater than the L_j/R time. (This is equivalent to $\beta_c > 1$ in the shunted junction model.[42]) For the junctions of the present system, that would require $C > \sim 10^{-15}$ F. However, an estimate of the junction capacitance, using an electrode separation of order 1 nm, gives a value $\sim 10^{-18}$ F, which is completely negligible. The other possible effect is due to charging effects of a single electron.[37] The characteristic energy $e^2/2C$ is indeed very large. However, this is screened by the other conduction electrons, as long as the junction resistance is much smaller than the characteristic quantum resistance $h/4e^2 \sim 6000\ \Omega$. Other research on similar NbN films has confirmed that the charging energy is significant only for films with sheet resistance on this order.[25] Finally, $J_c \sim 10^5 - 10^6$ A/cm^2 for our Josephson junctions, orders of magnitude larger than that for typical capacitively limited tunnel junctions. So our neglect of capacitive effects appears to be justified.

We have also neglected the effect of the ambient earth's magnetic field ~ 0.5 G on the sample characteristics. We point out in this regard that for a square Josephson junction array, a magnetic flux of $\Phi_0/2$ in each cell corresponds to a flux density of 10 kG for a lattice size $a \sim 30$ nm that is appropriate for this nanoscale granular material. This is the value of B that would be needed to completely suppress the supercurrent, corresponding to B_{c2} in the continuum limit. A field of 0.5 G is completely negligible here, until one gets to resistances some four orders of magnitude below the normal-state resistance (< 50 mΩ/square), where a residual flux-flow resistance would be present for large currents. So the results that we have reported here would be largely unchanged if magnetic shielding was used. In contrast, for a lattice scale of order 3 μm for the typical microfabricated Josephson junction array, the corresponding critical field is of order 1 G, so that shielding would be essential in that case.

Films similar to these ultrathin granular NbN lines have been proposed for a variety of possible applications including infrared photodetectors, rf inductors and delay lines, and broadband ''hot-electron'' bolometers.[31,36,43–45] The present study suggests that some of these devices, particularly if they are on the micron or submicron scale, may exhibit significant effects due to inhomogeneity in grain sizes and coupling.

In summary, we have studied the dc and rf electrical characteristics of a set of narrow lines of nanogranular NbN ultrathin superconducting films, in zero applied magnetic field. These are well described in terms of a regular array of 2D Josephson junctions, with lattice constant 32 nm, despite the highly disordered granular microstructure that is evident from AFM imaging. There is quantitative agreement of both resistive and inductive components with the standard theory of the Kosterlitz-Thouless vortex unbinding transition in such a regular array, with no adjustable parameters. Scaling of the nonlinear I-V characteristics below the transition indicate vortex pair creation and recombination within the film, even for very narrow lines where edge effects might be expected to be significant. An anomalous nonlinear kinetic inductance is observed, whereby L decreases with increasing I, counter to expectations of Ginzburg-Landau theory. We suggest that this may be due to ac effects in the Josephson array, as supported by preliminary numerical simulations. Finally, the microscopic inhomogeneity becomes evident in variations of the critical current and other critical parameters of the narrowest lines ($< 5\ \mu$m), as supported by a simple analytical model. In conclusion, this work suggests that the uniform junction model continues to maintain validity even for highly inhomogeneous junction distributions, provided that properties average out sufficiently on larger length scales.

ACKNOWLEDGMENTS

The authors would like to thank Michael Leung and James Murduck of TRW, Redondo Beach, CA, for designing, fabricating, and supplying the NbN samples. The AFM images were obtained courtesy of Lois Buitano and Jill Fornalik of Eastman Kodak Co., Rochester, NY. Some earlier parts of this work were carried out with the assistance of Andrea Herr. This research was supported in part by NSF Grant No. DMR-9122727 and Sigma Xi.

*Present address: TRW, Inc., Redondo Beach, CA 90278. Formerly also with Dept. of Physics and Astronomy, University of Rochester.

[1] D. J. Resnick, J. C. Garland, J. T. Boyd, S. Shoemaker, and R. S. Newrock, Phys. Rev. Lett. **47**, 1542 (1981).
[2] D. W. Abraham, C. J. Lobb, M. Tinkham, and T. M. Klapwijk, Phys. Rev. B **26**, 5268 (1982).
[3] C. J. Lobb, D. W. Abraham, and M. Tinkham, Phys. Rev. B **27**, 150 (1983).
[4] R. A. Webb, R. F. Voss, G. Grinstein, and P. M. Horn, Phys. Rev. Lett. **51**, 690 (1983).
[5] C. Leemann, P. Lerch, G. A. Racine, and P. Martinoli, Phys. Rev. Lett. **56**, 1291 (1986).
[6] S. E. Hebboul and J. C. Garland, Phys. Rev. B **43**, 13 703 (1991).
[7] T. P. Orlando, J. E. Mooij, and H. S. van der Zant, Phys. Rev. B **43**, 10 218 (1991).
[8] H. S. J. van der Zant, F. C. Fritschy, T. P. Orlando, and J. E. Mooij, Phys. Rev. B **47**, 295 (1993).
[9] S. G. Lachenmann, T. Doderer, D. Hoffmann, R. P. Huebener, P. A. Booij, and S. P. Benz, Phys. Rev. B **50**, 3158 (1994).
[10] M. Franz and S. Teitel, Phys. Rev. Lett. **73**, 480 (1994).
[11] Y. Cai, P. L. Leath, and Z. Yu, Phys. Rev. B **49**, 4015 (1994).
[12] H. A. Cerdeira and S. R. Shenoy, Physica B **222**, 253 (1996).
[13] M. G. Forrester, H. J. Lee, M. Tinkham, and C. J. Lobb, Phys. Rev. B **37**, 5966 (1988).
[14] M. B. Cohn, M. S. Rzchowski, S. P. Benz, and C. J. Lobb, Phys. Rev. B **43**, 12 823 (1991).
[15] P. Leath, Physica B **222**, 320 (1996).

[16] D. C. Harris, S. T. Herbert, D. Stroud, and J. C. Garland, Phys. Rev. Lett. **67**, 3606 (1991).
[17] C. Ebner and D. Stroud, Phys. Rev. B **28**, 5053 (1983).
[18] A. L. Eichenberger, J. Affolter, M. Willemin, M. Mombelli, H. Beck, P. Martinoli, and S. E. Korshunov, Phys. Rev. Lett. **77**, 3905 (1996).
[19] W. Y. Shih, C. Ebner, and D. Stroud, Phys. Rev. B **30**, 134 (1984).
[20] E. Granato and J. M. Kosterlitz, Phys. Rev. Lett. **62**, 823 (1986).
[21] D. Dominguez, Phys. Rev. Lett. **72**, 3096 (1994).
[22] P. L. Leath and W. Xia, Phys. Rev. B **44**, 9619 (1991).
[23] W. Xia and P. L. Leath, Phys. Rev. Lett. **63**, 1428 (1989).
[24] A. T. Fiory, A. F. Hebard, and W. I. Glaberson, Phys. Rev. B **28**, 5075 (1983).
[25] D. U. Gubser, S. A. Wolf, W. W. Fuller, D. Van Vechten, and R. W. Simon, Physica B **135**, 131 (1985).
[26] R. W. Simon, B. J. Dalrymple, D. Van Vechten, W. W. Fuller, and S. A. Wolf, Phys. Rev. B **36**, 1962 (1987).
[27] K. Epstein, A. M. Goldman, and A. M. Kadin, Phys. Rev. Lett. **47**, 534 (1981).
[28] A. M. Kadin, K. Epstein, and A. M. Goldman, Phys. Rev. B **27**, 6691 (1983).
[29] J. M. Murduck, J. DiMond, C. Dang, and H. Chan, IEEE Trans. Appl. Supercond. **3**, 2211 (1993).
[30] M. W. Johnson, A. M. Domino, and A. M. Kadin, IEEE Trans. Appl. Supercond. **3**, 2587 (1993).
[31] M. W. Johnson, A. M. Herr, and A. M. Kadin, J. Appl. Phys. **79**, 7069 (1996).
[32] M. W. Johnson, Ph.D. thesis, University of Rochester, 1996.
[33] H. Su, N. Yoshikawa, and M. Sugahara, Supercond. Sci. Technol. **9**, A152 (1996).
[34] J. R. Clem, B. Bumble, S. I. Raider, W. J. Gallagher, and Y. C. Shih, Phys. Rev. B **35**, 6637 (1987).
[35] Y. Imry and M. Strongin, Phys. Rev. B **24**, 6353 (1981).
[36] M. W. Johnson and A. M. Kadin, IEEE Trans. Appl. Supercond. **7**, 3492 (1997).
[37] M. Tinkham, *Introduction to Superconductivity*, 2nd ed. (McGraw-Hill, New York, 1996).
[38] M. R. Beasley, J. E. Mooij, and T. P. Orlando, Phys. Rev. Lett. **42**, 1165 (1979).
[39] B. I. Halperin and D. R. Nelson, J. Low Temp. Phys. **36**, 599 (1979).
[40] P. Minnhagen, Rev. Mod. Phys. **59**, 1001 (1987).
[41] S. Anlage, H. J. Snortland, and M. R. Beasley, IEEE Trans. Magn. **25**, 1388 (1989).
[42] T. Van Duzer and C. W. Turner, *Principles of Superconductive Devices and Circuits* (Elsevier, New York, 1981).
[43] K. R. Carroll, J. M. Pond, and E. J. Cukauskas, IEEE Trans. Appl. Supercond. **3**, 2808 (1993).
[44] K. Weiser, U. Strom, S. A. Wolf, and D. U. Gubser, J. Appl. Phys. **52**, 4888 (1981).
[45] G. N. Gol'tsman, A. D. Semenov, Y. P. Gousev, M. A. Zorin, I. G. Gogidze, E. M. Gershenzon, P. T. Lang, W. J. Knott, and K. F. Renk, Semicond. Sci. Technol. **4**, 435 (1991).